2

The Effect of Viscosity in Hypervelocity Impact Cratering

Robert W. MacCormack[1]

2.1 Abstract

A numerical method, of second order in both time and space, for the solution of the time-dependent compressible Navier-Stokes equations is presented. Conditions for stability are discussed. The method has been applied to calculate an axisymmetric flow field produced by hypervelocity impact. Results are given for impacts of aluminum cylinders (having diameters of 0.16, 0.32, and 0.64 cm) into aluminum targets. Viscosities of zero and 10^4 poise were assumed. Both plates and semi-infinite targets are considered at an impact speed of 10 km/sec. It is concluded that viscous effects become increasingly important as projectile size diminishes and cannot be neglected during the initial stages of crater formation for projectiles smaller than 0.5 cm in diameter.

2.2 Introduction

Denardo [1, 2] in 1964, reported a deviation from simple linear scaling in the hypervelocity impact of aluminum spheres, of diameters 0.16, 0.32, 0.64, and 1.27 cm, into aluminum targets. Penetration and momentum transfer

[1] NASA Ames Research Center, Moffett Field, California 94035.
This paper was originally presented as AIAA Paper 69-354 at the AIAA Hypervelocity Impact Conference in Cincinnati, Ohio. Permission of the AIAA to re-publish this classic paper in the present volume is gratefully acknowledged.
Frontiers of Computational Fluid Dynamics – 2002
Editors: David A. Caughey & Mohamed M. Hafez

to the target decreased more rapidly than simple scaling rules would imply as the projectile size was reduced. More explicitly, the ratios of penetration to projectile diameter and target momentum after impact to projectile momentum varied as the 1/18 and 1/6 powers, respectively, of projectile diameter. Two possible sources of this phenomenon are: (a) a pure scale effect in the static strength of the materials, as shown by Kuhn and Figge [3]; (b) a rate-dependent stress effect, for example, viscosity. The former would act toward the end of crater formation; the latter during the earlier part of crater formation where high shear rates exist. The purpose of this study is to observe the effect of viscosity during the initial stage of cratering (defined to take place from the initiation of impact until static strength effects become significant). During this time, hypervelocity impact cratering may be described by the Navier-Stokes equations of fluid dynamics, whose solutions scale nonlinearly for viscosities different from zero. A numerical method is described to solve these time-dependent equations. The method is of second order in both time and space, and is thus more accurate than the methods derived from the Los Alamos Particle In Cell Code [4], which have been previously used [5, 6, 7] to calculate hypervelocity impact phenomena. The results of the computation of several impact cases are examined to determine the effect of viscosity.

2.3 The Numerical Method

2.3.1 Differential Equations

The Navier-Stokes equations of fluid dynamics, neglecting body forces and heat sources, may be written [8]

$$\frac{\partial \rho}{\partial t} + \frac{\partial \rho u_j}{\partial x_j} = 0 \quad \text{(continuity equation)}$$

$$\frac{\partial \rho u_i}{\partial t} + \frac{\partial \rho u_i u_j}{\partial x_j} + \frac{\partial p}{\partial x_i} - \frac{\partial \sigma_{i,j}}{\partial x_j} = 0 \quad \text{(momentum equation)}$$

$$\frac{\partial e}{\partial t} + \frac{\partial (e+p)u_j}{\partial x_j} - \frac{\partial (u_i \sigma_{i,j} - q_j)}{\partial x_j} = 0 \quad \text{(energy equation)}$$

$$p = f(\epsilon, \rho) = f\left(\frac{e}{\rho} - \frac{|\vec{u}|^2}{2}, \rho\right) \quad \text{(equation of state)}$$

where Einstein notation has been used (repeated indices are summed) and

t = time

ρ = the mass per unit volume

u_i = component of velocity $\vec{u}$ in the x_i direction

$\sigma_{i,j}$ = viscous stress $= \lambda \delta_{i,j} \frac{\partial u_k}{\partial x_k} + \mu \left(\frac{\partial u_i}{\partial x_j} + \frac{\partial u_j}{\partial x_i} \right)$

where

$\delta_{i,j}$ = the Kronecker delta
μ, λ = first and second coefficients of viscosity, respectively
e = total energy per unit volume
$q_j = -k\frac{\partial T}{\partial x_j}$
where k is the coefficient of heat conductivity, and the temperature T and specific internal energy ϵ are related by an equation of form $\epsilon = g(\rho, T)$. Finally the pressure p is expressed as a function of ϵ and p.

This set of equations may easily be expressed in other coordinate systems [9]. A two-step difference method has been devised to numerically solve the above set. For simplicity and also to be consistent with descriptions of other numerical techniques in the literature, the method will be illustrated in a two-dimensional cartesian coordinate system. The application to an axisymmetric system will be briefly commented on later. Also, for the analysis of numerical stability only the inviscid non-heat-conducting equations will be treated in detail. Both the viscous and heat conduction terms, physically and also numerically (if their magnitudes in the differenced equations are not too great), tend to damp out the high frequency components of the solution. These components are normally the ones which cause numerical instability. Thus, the approach here of choosing μ and k equal to zero is conservative for the purposes of stability analysis. The equations in vector form are

$$\frac{\partial U}{\partial t} + \frac{\partial F}{\partial x} + \frac{\partial G}{\partial y} = 0 \tag{2.1}$$

where

$$U = \begin{pmatrix} \rho \\ m \\ n \\ e \end{pmatrix}, \quad F = \begin{pmatrix} m \\ m^2/\rho + p \\ mn/\rho \\ (e+p)m/\rho \end{pmatrix}, \quad G = \begin{pmatrix} n \\ mn/\rho \\ n^2/\rho + p \\ (e+p)n/\rho \end{pmatrix}$$

$$p = f(\epsilon, \rho) = f\left(\frac{e}{\rho} - \frac{m^2+n^2}{2\rho^2}, \rho\right)$$

and $m = \rho u$ and $n = \rho v$ are the momenta per unit volume in the x and y directions, respectively.

2.3.2 Difference Equations

The two-step difference method to solve Eq. (2.1) is defined by

$$\overline{U_{j,k}^{n+1}} = U_{j,k}^n - \frac{\Delta t}{\Delta x}\left(F_{j+1,k}^n - F_{j,k}^n\right) - \frac{\Delta t}{\Delta y}\left(G_{j,k+1}^n - G_{j,k}^n\right) \tag{2.2}$$

$$U_{j,k}^{n+1} = \frac{1}{2}\left\{U_{j,k}^n + \overline{U_{j,k}^{n+1}} - \frac{\Delta t}{\Delta x}\left(\overline{F_{j,k}^{n+1}} - \overline{F_{j-1,k}^{n+1}}\right) - \frac{\Delta t}{\Delta y}\left(\overline{G_{j,k}^{n+1}} - \overline{G_{j,k-1}^{n+1}}\right)\right\} \tag{2.3}$$

where $F^n_{j,k}$ and $G^n_{j,k}$ equal $F(U^n_{j,k})$ and $G(U^n_{j,k})$ respectively. The subscripts now and from here on refer to a spatial mesh of points (x_j, y_k) with spacing Δx and Δy, and the superscripts refer to times $t = n\Delta t$, where Δt is the time increment that the solution is advanced during each cycle of Eqs. (2.2,2.3). The method first obtains approximate values, $\overline{U^{n+1}_{j,k}}$ at each point, by Eq. (2.2), which uses two forward differences to approximate the two spatial derivatives. The approximate solution is then used to calculate $\overline{F^{n+1}_{j,k}}$ and $\overline{G^{n+1}_{j,k}}$, which are used in Eq.(2.3) with two backward differences to obtain the new accepted value $U^{n+1}_{j,k}$. As in the Particle In Cell method, the flow field can be viewed as divided into cells with forces acting on cell faces and with mass, momentum, and energy being transported between cells. The set of differential equations is in conservation law form [10]. Similarly, examination of the set of difference equations Eqs. (2.2,2.3), shows that mass, momentum, and energy are conserved during the calculation; that is, the differenced quantities in Eqs. (2.2,2.3) at interior points of the mesh appear exactly twice during a sweep through the mesh, each time of opposite sign. Thus, the vector sum, $\sum_{j,k} \overline{U^{n+1}_{j,k}}$ or $\sum_{j,k} U^{n+1}_{j,k}$ represents the net transport and stress effects at the boundaries.

2.3.3 Accuracy and Stability

The numerical stability of methods of this type, namely, those of Lax and Wendroff [10], cannot presently be completely analyzed in the general nonlinear form. The most successful attempt at analysis to date is to first linearize the set of differential Eqs. (2.1) and then to study the amplification of Fourier components of the solution by the difference method applied to the linearized set. The new set of equations is then

$$\frac{\partial U}{\partial t} + J_F \frac{\partial U}{\partial x} + J_G \frac{\partial U}{\partial y} = 0 \tag{2.4}$$

where J_F and J_G are the Jacobian matrices of F and G with respect to U and are considered to be constant.

$$J_F = \begin{pmatrix} 0 & 1 & 0 & 0 \\ -\frac{m^2}{\rho^2} + \frac{\partial p}{\partial \rho} & \frac{2m}{\rho} + \frac{\partial p}{\partial m} & \frac{\partial p}{\partial n} & \frac{\partial p}{\partial e} \\ -\frac{mn}{\rho^2} & \frac{n}{\rho} & \frac{m}{\rho} & 0 \\ -\frac{m}{\rho}\frac{e+p}{\rho} + \frac{m}{\rho}\frac{\partial p}{\partial \rho} & \frac{e+p}{\rho} + \frac{m}{\rho}\frac{\partial p}{\partial m} & \frac{m}{\rho}\frac{\partial p}{\partial n} & \frac{m}{\rho} + \frac{m}{\rho}\frac{\partial p}{\partial e} \end{pmatrix}$$

$$J_G = \begin{pmatrix} 0 & 0 & 1 & 0 \\ -\frac{mn}{\rho} & \frac{n}{\rho} & \frac{m}{\rho} & 0 \\ -\frac{n^2}{\rho^2} + \frac{\partial p}{\partial \rho} & \frac{\partial p}{\partial m} & \frac{2n}{\rho} + \frac{\partial p}{\partial n} & \frac{\partial p}{\partial e} \\ -\frac{n}{\rho}\frac{e+p}{\rho} + \frac{n}{\rho}\frac{\partial p}{\partial \rho} & \frac{n}{\rho}\frac{\partial p}{\partial m} & \frac{e+p}{\rho} + \frac{n}{\rho}\frac{\partial p}{\partial n} & \frac{n}{\rho} + \frac{n}{\rho}\frac{\partial p}{\partial e} \end{pmatrix}$$

$$\frac{\partial p}{\partial e} = \frac{\partial p}{\partial \epsilon}\frac{\partial \epsilon}{\partial e} = \frac{1}{\rho}\frac{\partial p}{\partial \epsilon}$$

$$\frac{\partial p}{\partial m} = \frac{\partial p}{\partial \epsilon}\frac{\partial \epsilon}{\partial m} = -\frac{m}{\rho^2}\frac{\partial p}{\partial \epsilon}$$

$$\frac{\partial p}{\partial n} = \frac{\partial p}{\partial \epsilon}\frac{\partial \epsilon}{\partial n} = -\frac{n}{\rho^2}\frac{\partial p}{\partial \epsilon}$$

$$\frac{\partial p}{\partial \rho} = \left.\frac{\partial p}{\partial \rho}\right|_{\epsilon} + \frac{\partial p}{\partial \epsilon}\frac{\partial \epsilon}{\partial \rho} = \left.\frac{\partial p}{\partial \rho}\right|_{\epsilon} + \left(-\frac{e}{\rho^2} + \frac{m^2+n^2}{\rho^2}\right)\frac{\partial p}{\partial \epsilon}$$

The set of Eqs. (2.4) approximates Eq. (2.1) locally, and difference methods found unstable on it can be expected to be unstable in the general nonlinear case. Two conditions inherent in such an analysis are: (a) the boundary conditions have no effect on stability, and (b) the exact solution to Eq. (2.1) is smooth. The latter condition allows the matrices J_F and J_G to be treated as constant. The results of the analysis thus apply principally to regions of the flow away from the boundaries and in which there are no discontinuities, such as shock waves. In the next few paragraphs, this method of analysis will be used to obtain a bound for the maximum amplification of any Fourier component of the solution in regions which satisfy these conditions.

The amplification matrix of the present method applied to Eq. (2.4) for a single Fourier component of the solution,

$$W(t)\exp[i(k_1 x + k_2 y)]$$

becomes [11],

$$\begin{aligned} G = I + \quad & i\tfrac{\Delta t}{\Delta x}\left(J_F \sin\xi + J_G \sin\eta\right) \\ & -\tfrac{1}{2}\left(\tfrac{\Delta t}{\Delta x}\right)^2 \left(\left(1-e^{-i\xi}\right)J_F + \left(1-e^{-i\eta}\right)J_G\right) \\ & \left(\left(1-e^{i\xi}\right)J_F + \left(1-e^{i\eta}\right)J_G\right) \end{aligned} \tag{2.5}$$

where $\xi = k_1\Delta x$, $\eta = k_2\Delta y$, and equal spacing is assumed ($\Delta x = \Delta y$).

For ξ and $\eta \ll 1$, the approximations $\sin\xi = \xi$, $1 - \cos\xi = \xi^2/2$, and $1 + \cos\xi = 2 - \xi^2/2$ and similar ones for η may be used to show that

$$G = I + i\frac{\Delta t}{\Delta x}\left(J_F\xi + J_G\eta\right) - \frac{1}{2}\left(\frac{\Delta t}{\Delta x}\right)^2 \left(J_F\xi + J_G\eta\right)^2 + O(\xi^3, \eta^3)$$

Thus $G = \exp\left[i\frac{\Delta t}{\Delta x}(J_F\xi + J_G\eta)\right]$ modulo terms of third order in ξ and η. The exact solution of the differential Eq. (2.4) for the above Fourier component is

$$\exp[it(k_1 J_F + k_2 J_G)]\exp[i(k_1 x + k_2 y)]W(0)$$

Hence, the exact amplification of the solution from $t = 0$ to $t = \Delta t$ is

$$\exp[i\Delta t(k_1 J_F + k_2 J_G)] = \exp\left[i\frac{\Delta t}{\Delta x}(J_F\xi + J_G\eta)\right]$$

The difference between the two is of third order in ξ and η. Thus, the method defined by Eqs. (2.2,2.3) is of second order accuracy [10].

G may also be written as

$$G = I + M - M^* - 2M^*M$$

where

$$M = \frac{1}{2}\frac{\Delta t}{\Delta x}\left(\left(1 - e^{i\xi}\right)J_F + \left(1 - e^{i\eta}\right)J_G\right)$$

and M^* is the complex conjugate of M.

Stability is assured if it can be shown that all of the eigenvalues λ_i of G satisfy the von Neumann condition $|\lambda_i| \leq 1 + O(\Delta t)$ [11]. The eigenvalues of G are invariant under a similarity transformation. Using such a transformation S, M may be written as

$$M = S\frac{1}{2}\frac{\Delta t}{\Delta x}\left(\left(1 - e^{i\xi}\right)A + \left(1 - e^{i\eta}\right)B\right)S^{-1}$$

where

$$A = \begin{pmatrix} u & c & 0 & 0 \\ c & u & 0 & 0 \\ 0 & 0 & u & 0 \\ 0 & 0 & 0 & u \end{pmatrix}$$

$$B = \begin{pmatrix} v & 0 & c & 0 \\ 0 & v & 0 & 0 \\ c & 0 & v & 0 \\ 0 & 0 & 0 & v \end{pmatrix}$$

$$S^{-1} = \begin{pmatrix} c & 0 & 0 & \beta/c \\ 0 & 1 & 0 & 0 \\ 0 & 0 & 1 & 0 \\ 0 & 0 & 0 & 1 \end{pmatrix}\begin{pmatrix} 1 & 0 & 0 & 0 \\ -u & 1 & 0 & 0 \\ -v & 0 & 1 & 0 \\ -\alpha & -u & -v & 1 \end{pmatrix}$$

$$S = \begin{pmatrix} 1 & 0 & 0 & 0 \\ u & 1 & 0 & 0 \\ v & 0 & 1 & 0 \\ u^2 + v^2 + \alpha & u & v & 1 \end{pmatrix}\begin{pmatrix} 1/c & 0 & 0 & -\beta/c^2 \\ 0 & 1 & 0 & 0 \\ 0 & 0 & 1 & 0 \\ 0 & 0 & 0 & 1 \end{pmatrix}$$

where

$$c^2 = \frac{\partial p}{\partial \rho}\Big)_{\epsilon} + \frac{p}{\rho^2}\frac{\partial p}{\partial \epsilon},$$

is the square of the local adiabatic speed of sound,

$$\alpha = \frac{e+p}{\rho} - u^2 - v^2$$

and

$$\beta = \frac{1}{\rho}\frac{\partial p}{\partial \epsilon}$$

Then $G' = S^{-1}GS = I + M' - M'^* - 2M'^*M'$, where $M' = S^{-1}MS$ and is symmetric.

For any unit vector w, the inner product

$$\begin{aligned}(w, G'w) &= (w,w) + (w, M'w) - (w, M'^*w) - 2(w, M'^*M'w) \\ &= 1 - 2\|M'w\|^2 + (w, M'w) - (w, M'^*w)\end{aligned}$$

where the norm of $M'w$ is denoted by $\|M'w\| = (M'w, M'w)^{1/2}$.

The quantity $(w, M'w) - (w, M'^*w)$ is pure imaginary and since

$$|(w, M'w)| \leq \|w\|\|M'w\| = \|M'w\|$$

by the Cauchy-Schwartz inequality

$$|(w, G'w)|^2 \leq (1 - 2\|M'w\|^2)^2 + (2\|M'w\|)^2 \leq 1 + 4\|M'w\|^4$$

Gerschgorin's theorem [12] may be used to show

$$\|M'w\| \leq \frac{\Delta t}{\Delta x}(|u| + |v| + 2c)$$

Thus, if $\nu = 4\frac{\Delta t^3}{\Delta x^4}(|u| + |v| + 2c)^4 \approx 1$ then $|(w, G'w)| \leq 1 + \nu O(\Delta t)$. If, in particular, w is any eigenvector of G', $G'w = \lambda w$. Then

$$|\lambda|^2 \leq 1 + \nu\Delta t$$

or

$$|\lambda| \leq 1 + O(\Delta t)$$

Hence, all the eigenvalues of G satisfy $|\lambda_i| \leq 1 + O(\Delta t)$ if ν is of the order of unity.

That is, if ν is held constant as Δt, $\Delta x \to O$, and Eqs. (2.2,2.3) are used to calculate the solution to time T, the number n of time steps is $T/\Delta t$ and the amplification of any Fourier component is then less than

$$\sup_{\text{All w, } (w,w)=1} |(w, Gw)|^n \leq (1 + \nu\Delta t)^{n/2} \leq e^{(n/2)\nu\Delta t} = e^{\nu T/2}$$

The amplification of every component of the solution can thus be made arbitrarily small, in computing to a given time by suitably choosing ν.

In one dimension (i.e., $U = \begin{pmatrix} \rho \\ m \\ e \end{pmatrix}$, $F = \begin{pmatrix} m \\ m^2/\rho + p \\ (e+p)m/\rho \end{pmatrix}$, and $G = 0$) it is easily shown that the eigenvalues of the amplification matrix of the method are less than unity if $\frac{\Delta t}{\Delta x}(|u| + c) \leq 1$. This condition is the well-known Courant-Friedrichs-Lewy (C.F.L.) condition that often appears in fluid dynamics. This is the best bound that can be realized in numerical methods. The noncommutativity of the matrices A and B has presently prevented the calculation of the eigenvalues for two dimensions. The condition, $\frac{\Delta t}{\Delta x}(|u| + |v| + 2c) \approx \Delta t^{1/4}$, obtained from the derived bound is substantially more restrictive than the two-dimensional C.F.L. condition. Although it can be shown that the derived eigenvalue bound is not the least upper bound, it also can be shown that an eigenvalue does exist such that a more restrictive condition than the C.F.L. condition is required for stability. However, the method defined by Eqs. (2.2,2.3) is only one of four methods of second order accuracy of essentially the same form. For example, if instead of first using two forward spatial differences and then two backward differences, the reverse procedure could be followed, or one forward and one backward difference could be followed by corresponding backward and forward differences. The amplification matrix of each would have different eigenvalues and eigenvectors for the same Fourier component of the solution. Thus if the indices of the method defined by Eqs. (2.2,2.3) were permuted so that the four methods followed one another cyclically, a smaller amplification would be expected; that is, although the maximum eigenvalue in magnitude $|\lambda_{\max}(G_i)|$ for each G_i, maximized on the set of all ξ, η, u and v, such that $|u| + |v| \leq$ constant and c is constant would be the same, a single choice of ξ, η, u and v would not in general maximize all G_i (i.e., $|\lambda_{\max}(G_1G_2G_3G_4)| \leq |\lambda_{\max}(G_i)^4$, $i = 1$, 2, 3 and 4). It is conjectured that $|\lambda_{\max}(G_1G_2G_3G_4)| \leq 1 + O(\Delta t)$ if Δt and Δx satisfy a condition close to the C.F.L. condition.

As previously stated, the addition of viscous and heat conduction terms does not disturb the numerical stability if their magnitudes are not too great (that is, if Δt and Δx are chosen so that $\frac{\mu}{\rho}\frac{\Delta t}{\Delta x^2}$, $k\frac{\Delta t}{\Delta x^2}$ are sufficiently less than one). Second-order accuracy will also be maintained if the terms are differenced so that their truncation error is also of second order. For example, the viscous term $\frac{\partial \mu\left(\frac{\partial u}{\partial x}\right)}{\partial x}$, if differenced centrally,

$$\frac{\left(\frac{\mu_{i+1}+\mu_i}{2}\frac{u_{i+1}-u_i}{\Delta x} - \frac{\mu_i+\mu_{i-1}}{2}\frac{u_i-u_{i-1}}{\Delta x}\right)}{\Delta x}$$

or if μ is constant

$$\mu\frac{u_{i+1} - 2u_i + u_{i-1}}{\Delta x^2}$$

will suffice for second-order accuracy.

The stability analysis is also essentially the same in axisymmetric cylindrical coordinates. For example, the set of equations corresponding to Eq. (2.4) is

$$\frac{\partial U}{\partial t} + J_F \frac{1}{r}\frac{\partial rU}{\partial r} + J_G \frac{\partial U}{\partial z} = J_H \frac{U}{r} \tag{2.6}$$

where r and z are the radial and axial coordinates, J_F, J_G and U are the corresponding matrices and vector defined in these coordinates and J_H is the Jacobian of H, $H^T = (0, p, 0, 0)$, with respect to U. In flow regions away from the axis, $r \gg \Delta r$, it can be shown that the effect of deleting the term $J_H \frac{U}{r}$ from Eq. (2.6) causes a change in the eigenvalues of the associated amplification matrix of only the order of Δt. Thus, to analyze the stability of the difference method applied to Eq. (4) in regions away from the axis, the right hand side of Eq. (4) may be set to the zero vector. The Fourier component of the solution for this equation with the same wave numbers k_1 and k_2 as considered earlier is

$$\frac{1}{r}\exp[it(k_1 J_F + k_2 J_G)]\exp[i(k_1 r + k_2 z)]$$

Similarly, the corresponding component of the solution to the difference equations, where $\frac{1}{r}\frac{\partial rU}{\partial r}$ is forward differenced as

$$\frac{1}{(i-1/2)\Delta r}\frac{(i+1/2)\Delta r U_{i+l,j} - (i-1/2)\Delta r U_{i,j}}{\Delta r}$$

and backward differenced as

$$\frac{1}{(i-1/2)\Delta r}\frac{(i-1/2)\Delta r U_{i,j} - (i-3/2)\Delta r U_{i-1,j}}{\Delta r}$$

is

$$\frac{1}{r}W(t)\exp[i(k_1 r + k_2 z)]$$

The amplification matrix for this component by Eq. (2.6), after differencing, is the same as obtained earlier, except that now x and y are replaced by r and z. Near the axis $r = 0$, the boundary conditions induced by axial symmetry (i.e., $u_{1,j} = -u_{-1,j}$, $v_{1,j} = v_{-1,j}$, $p_{1,j} = p_{-1,j}$, etc.) are expected to influence stability, and the above linearized analysis is thus not sufficient. The numerical stability in this region has not yet been analyzed. Also, the nonzero component of H, occurring from the radial momentum equation, does not allow the equations to be expressed in divergence form [13]. Thus, the difference method applied to Eq. (2.6) rigorously conserves only mass, axial momentum and energy and not radial momentum as well. Again the second-order terms of the differential equations are not expected to disturb the numerical stability and if also differenced to second-order accuracy, the

method itself will be of second-order accuracy. For example, differencing the term $\frac{1}{r}\frac{\partial r\mu(\partial u/\partial r)}{\partial r}$ by

$$\frac{i\Delta r\left(\frac{\mu_{i+1,j}+\mu_{i,j}}{2}\right)\left(\frac{u_{i+1,j}-u_{i,j}}{\Delta r}\right)-(i-1)\Delta r\left(\frac{\mu_{i,j}+\mu_{i-1,j}}{2}\right)\left(\frac{u_{i,j}-u_{i-1,j}}{\Delta r}\right)}{(i-1/2)\Delta r\cdot\Delta r}$$

will preserve accuracy.

The advantage of the described method in comparison to the Particle In Cell method is its second-order accuracy. The necessity of using a method of greater accuracy than first order in computing hypervelocity impact problems which include the effect of viscosity will be discussed in the Numerical Calculations. The advantages in comparison to others of second-order accuracy [10, 11, 13, 14] are: (a) The extension to any Eulerian coordinate system is straightforward; (b) The calculation to advance the solution at one point, for the inviscid difference Eqs. (2.2,2.3), requires knowledge of only seven neighboring points, rather than the usual nine; (c) If the mesh is swept row-wise (x direction) and the solution is modified only by the differences in the x direction, say, $\frac{\Delta t}{\Delta x}(F_{j+1,k}-F_{j,k})$, then for each j only $F_{j+1,k}$ need be calculated since $F_{j,k}$ is known from the previous calculation at "cell$_{j-1,k}$". Similarly, after completion of this sweep, the mesh is then swept column-wise to account for the difference terms in the y direction, again computing and saving the values of the transport, stress, and conduction terms at only one "cell face" for each k, and hence reducing the amount of computation significantly. This procedure could be followed to differing extents by other Lax-Wendroff methods, some requiring the values at two previous cell faces to be saved and others able to use again only parts of the calculation at each face. The disadvantage of the method is that the eigenvalues of the amplification matrix, as discussed above, are not known. If the restriction on Δt necessary to fulfill the von Neumann condition is severe, the efficiency gained by advantages (b) and (c) may be more than offset in some problems.

For the problems considered in this paper Δt was simply chosen to be the smaller of the two values $\frac{1}{3}\frac{\Delta x}{v_p}$ and $\frac{\rho_0}{8}\frac{\Delta x^2}{\mu}$, where v_p is the projectile impact velocity and ρ_0 is the initial density. With this choice and with no permutation of the indices of the method defined by Eqs. (2.2,2.3), no sign of numerical instability was observed. Each problem, with a computational mesh of 32 × 33 cells, took about 130 time-steps to complete. The machine time was approximately 15 minutes on the IBM 7094.

2.4 Numerical Calculations

The method defined by Eqs. (2.2,2.3) was applied to solve the Navier-Stokes equation for a compressible, non-heat-conducting viscous fluid in cylindrical coordinates. The hydrostatic pressure was assumed equal to the average normal stress (i.e., the "second coefficient of viscosity" was set equal to -2/3 the "first coefficient." See Ref. 15). The solutions of these equations do not scale linearly with characteristic size as do their inviscid counterparts. However if a solution for one characteristic size d and viscosity μ is obtained, then all solutions of characteristic size and viscosity d' and μ' such that $\frac{\mu'}{d'} = \frac{\mu}{d}$ are known, all other parameters being kept equal. That is, time t, distance and viscosity scale as

$$t \to st$$
$$d \to sd$$

and

$$\mu \to s\mu$$

where s is any real number.

Thus, the particular choice of μ is not as important as the choice of the ratio $\frac{\mu}{d}$.

For all cases studied the projectile was an aluminum right circular cylinder of length equal to its diameter impacting an aluminum target at a velocity of 1 cm/μsec. The equation of state used in the calculations was that formulated by Tillotson [16] for aluminum. Sakharov [17] deduced from shock-wave experiments that the coefficient of viscosity μ of an aluminum alloy (90% Al) at 0.3 Mb (megabar) was approximately 0.02 Mp (megapoise) and increased weakly, but did not exceed 0.1 Mp for shock pressures up to 1 Mb. For this paper a constant value of 0.01 Mp was assumed to be representative of the values of μ during the compressive phases, from the initial impact at which the shock pressure was 1.54 Mb until the calculations ceased and the shock had attenuated to approximately an order of magnitude greater than the material strength of aluminum (2 or 3 kb). As previously stated, the particular choice of μ is not as important as the ratio $\frac{\mu}{d}$ and the results for the chosen value of μ may be scaled to any other choice. During the calculations, regions of expansion were treated as inviscid flows. More explicitly, when ρ became less than $\rho_0/1.1$, where ρ_0 is the initial density, μ was set to zero.

The chosen value of μ was, in general, of the same order numerical magnitude as the mesh spacing Δx. The magnitude of the viscous stress terms is then proportional to Δx, while that of the truncation error for the method of second-order accuracy, described in the last section, is proportional to Δx^2. Thus, if a method of only first-order accuracy were used, namely, the Particle In Cell Code, with the same mesh spacing, the viscous stress and truncation

error would be of the same order of magnitude. A mesh spacing, say, $\Delta x \approx \mu^2$, chosen to insure that the viscous stress is dominant in comparison with the truncation error is impractical $\left(\Delta t \approx \frac{\Delta x^2}{\mu} \approx \mu^3\right)$. Also, there is a danger that the stability of the Particle In Cell method would be destroyed by such a choice (i.e., the terms introduced by truncation in P.I.C. themselves act viscously). Therefore, because of the order of magnitude of the coefficient of viscosity of aluminum, a method of at least second-order accuracy is necessary.

The computational mesh was re-zoned $\Delta x \to 2\Delta x$ and $\Delta y \to 2\Delta y$) each time the target shock wave or ejecta approached the mesh boundaries.

At intervals during each calculation the total positive component of axial momentum Z_+ and the total radial momentum R were determined. That is,

$$Z_+ = \sum_{\text{Cells with } u_{i,j}>0} \rho_{i,j} u_{i,j} (\text{cell volume})_{i,j}$$

and

$$R = \sum_{\text{All cells}} \rho_{i,j} v_{i,j} (\text{cell volume})_{i,j}$$

The total negative component of axial momentum Z_- is, by conservation of momentum, equal to $mv_p - Z_+$, where mv_p is the projectile momentum. To be precise R, unlike Z_+ and Z_-, is not a vector since the quantities $\rho_{i,j} v_{i,j} (\text{volume of cell})_{i,j}$ have been summed algebraically. The vector sum would vanish because of the axial symmetry.

2.4.1 Semi-Infinite Targets

The impact into thick targets of projectiles of diameters 0.16, 0.32, and 0.64 cm with $\mu = 0.01$ Mp and, for comparison, with $\mu = 0$, was studied to determine if a momentum scale effect, comparable to that observed experimentally, could be caused by viscosity. The values for Z_+ and R normalized by the initial projectile momentum are shown in Fig. 1 versus the nondimensional time τ, where $\tau = v_p \frac{t}{d}$. The effect of viscosity is clearly shown here by each impact case having a distinct curve. It is also observed that at late times Z_+ and R for each case increase nearly linearly. Fig. 2 shows the relationship of Z_+ and R to d for $\tau = 8$, a time near the end of computation. Quantitatively, the scale effect is displayed here by the slopes of the curves, different from zero for both Z_+ and R. The slope is seen to increase slightly for both curves as d decreases. For example, the slope of a straight line through the points of Z_+ at $d = 0.32$ cm and at 0.64 cm is 0.113, and that for $d = 0.16$ cm and 0.32 cm is 0.146. Similarly, the corresponding slopes for the curve for R are 0.082 and 0.1126. These values are typical of those near the end of computation and do not appear to be changing appreciably. It is to be stressed that Z_+ is not the same quantity measured experimentally as target momentum. The target during the

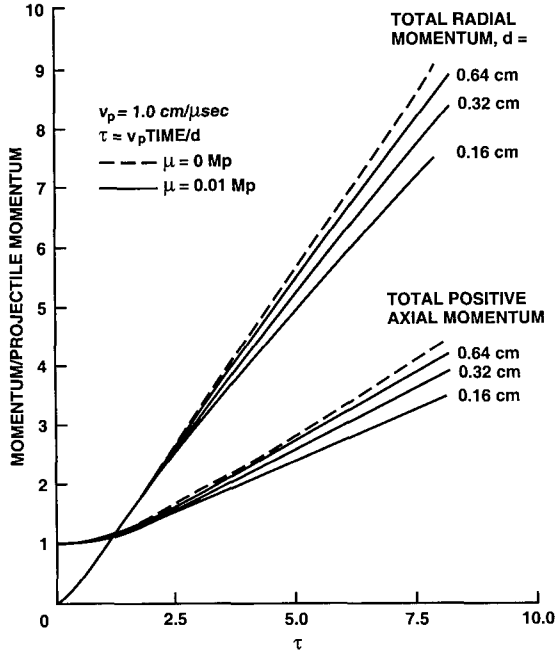

Figure 1 Momentum versus τ for $d = 0.16$, 0.32, and 0.64 cm

calculation was observed to contain large amounts of positive axial momentum near the axis and also appreciable amounts of negative axial momentum in the region forming the crater lip. The net effect would be the momentum of the target. Nevertheless the observed deviation from simple linear scaling in momentum in the numerical calculations would be expected to be reflected in the experimental measurements. The diameter exponents (slopes of the curves of Fig. 2) are somewhat lower than those found by experiment for spherical projectiles in approximately the same size range. The change in slope of both curves is an indication that the exponent of d depends on μ/d, and a better correlation with experiment would be expected for a somewhat larger value of μ at the same reported values of d. Also a greater deviation from simple linear scaling is to be expected in the momentum measurements of micometeoroids than that of laboratory-sized projectiles.

2.4.2 Finite Targets

The effect of viscosity in the impact of thin-sheet targets was also investigated. In each case the projectile diameter was 0.16 cm and the impact velocity was

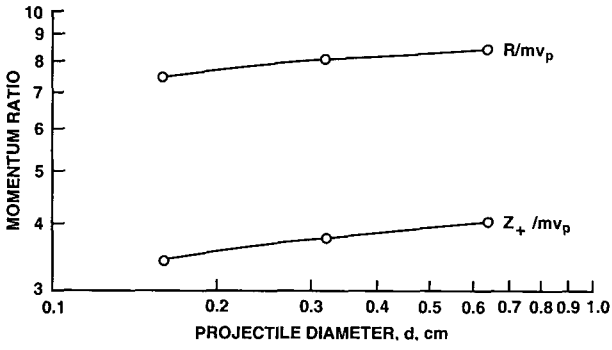

Figure 2 Momentum ratios of total positive axial momentum Z_+ and total radial momentum R to projectile momentum mv_p versus projectile diameter d at nondimensional time $\tau = 8$

1.0 cm/μsec. The momentum results for the impact of sheets of thickness th equal to 0.08, 0.16, and 0.24 cm are shown in Figs. 3(a) and (b). The most significant feature is the large attenuation of total positive axial momentum caused by viscosity in comparison with that of total radial momentum. In fact, for the cases of $th/d \leq 1$ there is little or no reduction in R. The expected consequence of the greater attenuation in axial momentum, because of viscosity, is that the momentum of the spray, composed of both projectile and target material, moving through the impacted sheet, will be less intense and more divergent and thus will be less damaging to any subsequently impacted structure.

For finite targets, the impact process, because of the rapid attenuation of pressure caused by free surfaces, is expected to be dominated by the initial fluid dynamic stage. A finite-target scale effect found experimentally in spray-momentum measurements and in the solid angles in which the spray is distributed would add convincing evidence that the scale effect found in semi-infinite targets is caused by viscosity. Conversely, the absence of such an effect would lend credence to theory that the semi-infinite target scale effect is caused during the later, strength-dependent stages.

2.5 Concluding Remarks

1. Though it has not been shown conclusively that the scale effect found experimentally in semi-infinite targets is caused by viscosity, it has been shown that the total positive axial and radial momentum during the initial stages of cratering exhibit an effect, caused by expected levels of viscosity, consistent

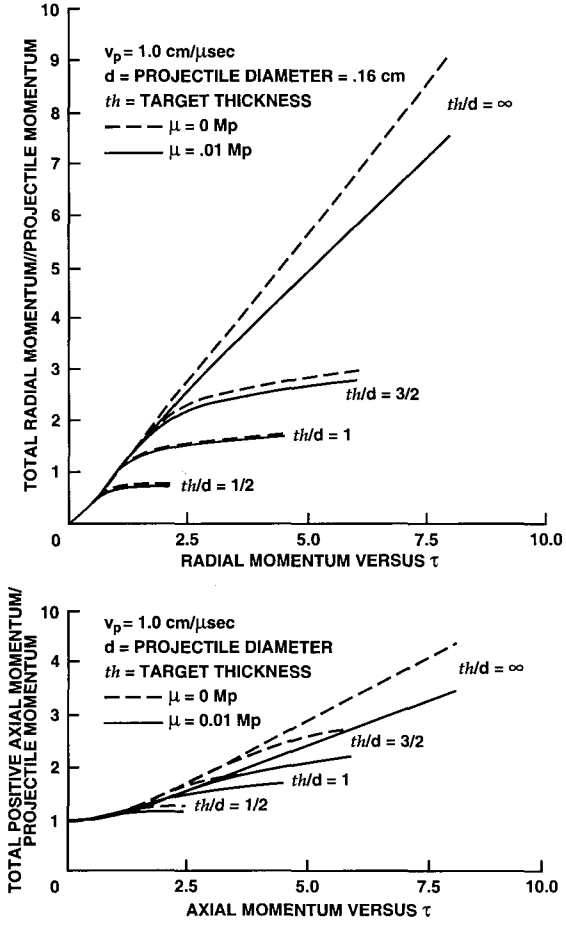

Figure 3 Momentum versus τ for $th/d = 1/2$, 1, and 3/2

with experimental momentum measurements. It is expected that this effect will become increasingly important as projectile size diminishes.

2. Viscosity in thin targets is expected to reduce the momentum of the spray passing through the perforated target. An experimental study, in which the projectile-thin sheet geometry is unchanged as size is varied, could confirm the importance of viscosity in hypervelocity impact and provide an approach to the experimental evaluation of effective viscosity under the conditions of hypervelocity impact.

REFERENCES

1. Denardo, B. Pat & Nysmith, C. Robert, Momentum Transfer and Cratering Phenomena Associated with the Impact of Aluminum Spheres into Thick Aluminum Targets at Velocities to 24,000 Feet Per Second. AGARDograph 87, vol. 1. Gordon and Breach, Science Publishers, New York, 1966.
2. Denardo, B. Pat, Summers, James L. & Nysmith, C. Robert, Projectile Size Effects on Hypervelocity Impact Craters in Aluminum. **NASA TN D-4067**, 1967.
3. Kuhn, Paul & Figge, I. E., Unified Notch-Strength Analysis for Wrought Aluminum Alloys. **NASA TN D-1259**, 1962.
4. Rich, Marvin & Blackman, Samuel S., A Method for Eulerian Fluid Dynamics. Los Alamos Scientific Laboratory, **LAMS-2826**, 1963.
5. Walsh, J. M., Johnson, W. E., Dienes, J. K., Tillotson, J. H. & Yates, D. R., Summary Report on the Theory of Hypervelocity Impact. General Atomic, Div. of General Dynamics, **GS-5119**, 1964.
6. Riney, T. D., Theoretical Hypervelocity Impact Calculations Using the PICWICK Code. General Electric, **R64SD13**, 1964.
7. Bjork, R. L., Kreyenhagen, K. N. & Wagner, M. H., Analytical Study of Impact Effects as Applied to the Meteoroid Hazard. Shock Hydrodynamics, Inc., 1966.
8. Liepmann, H. W. & Roshko, A., **Elements of Gasdynamics**. John Wiley and Sons, 1957.
9. Walkden, F., The Equations of Motion of a Viscous, Compressible Gas Referred to an Arbitrary Moving Co-ordinate System. Royal Aircraft Establishment, England, **Tech. Rep. 66140**, 1966.
10. Lax, Peter D. & Wendroff, Burton, Difference Schemes for Hyperbolic Equations with High Order of Accuracy. **Comm. Pure and Appl. Math.**, vol. XVII, 1964, pp. 381-398.
11. Richtmyer, Robert D. & Morton, K. W., **Difference Methods for Initial Value Problems**. Second ed. Interscience Publishers, 1967.
12. Isaacson, Eugene & Keller, Herbert, **Analysis of Numerical Methods**. John Wiley and Sons, 1966.
13. Burstein, Samuel Z., Finite-Difference Calculations for Hydrodynamic Flows Containing Discontinuities. **J. Comp. Phys.**, 2, 1967.
14. Rubin, Ephraim L. & Burstein, Samuel Z., Difference Methods for the Inviscid and Viscous Equations of a Compressible Gas. **J. Comp. Phys.**, 2, 1967.
15. Pai, Shih-I, **Viscous Flow Theory**. D. Van Nostrand Co., New York, 1956.
16. Tillotson, J. H., Metallic Equations of State for Hypervelocity Impact. General Atomic, Div. of General Dynamics, **Rep. GS-3216**, 1962.
17. Sakharov, A. D., Zaidel, R. M., Miniev, V. N., & Oleinik, A. G., Experimental

Investigations of the Stability of Shock Waves and the Mechanical Properties of Substances at High Pressures and Temperatures. Soviet Physics, Doklady, Vol. 9, No. 12, June 1965, p. 1091.